

Semiconductivity, spin delocalization, and excited states of the single molecule magnets Fe_8Br_8 and Mn_{12} -acetate (invited)

D. Zipse,^{a)} J. M. North, R. M. Achey, and N. S. Dalal

Department of Chemistry and Biochemistry and National High Magnetic Field Laboratory, Florida State University, Tallahassee, Florida 32306

S. Hill and R. S. Edwards

Department of Physics, University of Florida, Gainesville, Florida 32611

E. S. Choi and J. S. Brooks

National High Magnetic Field Laboratory, Florida State University, Tallahassee, Florida 32306

(Presented on 7 January 2004)

Some newly found properties of the single-molecule magnets Mn_{12} -acetate and Fe_8Br_8 are summarized: they are semiconductors and their 20 unpaired ($S=10$) electrons are delocalized not only on the metal ions, but also quite significantly (several percent) on the organic linkers (ligands). Fe_8Br_8 has an $S=9$ excited state located at about 24 K (17 cm^{-1}) above the $S=10$ ground state. The zero-field (D and E) parameters of the $S=9$ state differ from those of the $S=10$ state by 7%–8%. The band gap for Mn_{12} -acetate was found to be 0.37 eV, while that for Fe_8Br_8 was 0.73 eV. Details of the experimental techniques used (EPR, NMR, isotope-labeling, four-point conductivity) are provided, together with the discussions of the results in the context of other experimental techniques, and theoretical calculations. © 2004 American Institute of Physics.

[DOI: 10.1063/1.1664451]

I. INTRODUCTION

Compounds that have come to be known as single molecule magnets, (SMMs),^{1,2} have lately been the focus of intensive research due to their novel properties, such as macroscopic quantum tunneling,^{3–6} and hysteresis loops at a single-molecule level.⁷ SMMs are thus considered to be candidates for magnetic memory at molecular dimensions,^{8,9} and elements of quantum computing.¹⁰ While considerable progress has been made in the understanding of these materials, questions remain regarding their spin exchange constants (J s), exact spin Hamiltonians, excited states and spin density distribution over the entire molecular framework, and charge transport properties (crucial for electro-optic applications). Two of the best characterized SMMs are



abbreviated as $\text{Mn}_{12}\text{-Ac}$,¹¹ and



henceforth Fe_8Br_8 .¹² This presentation attempts to summarize our recent progress related to all three aspects for both of these SMMs.

II. MATERIALS AND METHODS

A. Sample preparation

$\text{Mn}_{12}\text{-Ac}$ single crystals in dimensions of about $0.5 \times 0.5 \times 3.0\text{ mm}^3$ were grown using the method outlined by Lis.¹¹ Fe_8Br_8 was synthesized according to Weighardt.¹² Relatively large ($2\text{ mm} \times 2\text{ mm} \times 0.5\text{ mm}$) single crystals were grown by slow evaporation over several days. The samples were checked through x-ray crystallography, and magnetization measurements to ensure the integrity of the sample.

B. Nuclear magnetic resonance measurements

⁸¹Br NMR measurements were carried out on a large single crystal of Fe_8Br_8 in a 8.5406 T magnetic field with sample orientations spanning the intermediate to hard magnetic axes. ¹³C NMR measurements were carried out on $\text{Mn}_{12}\text{-Ac}$ samples that were isotopically labeled with ¹³C at the methyl and carbonyl carbon sites, as described earlier.^{13,14} Isotopically labeled samples were prepared by substituting the appropriately labeled acetic acid in the standard synthesis. The samples acquired were ground into powder and mixed with Stycast 1266 epoxy, then placed in an 8.5 T magnetic field to produce magnetically aligned samples. The NMR spectrometer used has been developed at the National High Magnetic Field Laboratory and described elsewhere.¹⁵

^{a)}Electronic mail: dzipse@chem.fsu.edu

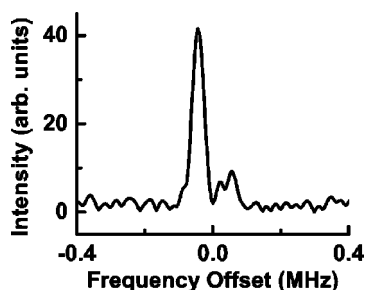


FIG. 1. ^{81}Br NMR spectrum of Fe_8Br_8 at 280 K, with a frequency offset of 0.0 MHz corresponding to the Larmor frequency of 98.1988 MHz. The large peak has been assigned to the seven bound bromines in the Fe_8Br_8 crystal structure, while the smaller peak corresponds to the unbound bromine.

C. Electron paramagnetic resonance measurements

The EPR measurements were made using a variable frequency (44–200 GHz), cavity-based, high-sensitivity spectrometer described earlier.¹⁶ The primary component of the spectrometer is a millimeter-wave vector network analyzer (MVNA), a phase sensitive, fully sweepable, superheterodyne source/detection system. A variable flow cryostat situated within the bore of a 17 T magnet allows for temperatures down to 1.5 K, within an accuracy of ± 0.01 K. The high sensitivity of the MVNA technique (10^9 spins $\text{G}^{-1} \text{s}^{-1}$) enables the observations of low level transitions of the Fe_8Br_8 ground and excited states in a single crystal.

D. Conductivity

dc conductivity measurements were made in a constant voltage or current configuration using a standard four probe technique. A high input impedance electrometer was used to measure the voltage drop across the sample when constant current was applied. Typically, the voltages used were 100 V or less, and the currents were in the 0.1–10 nA range. All measurements were made under vacuum in a temperature controlled probe.

III. SPIN DELOCALIZATION MEASUREMENTS

A. ^{81}Br nuclear magnetic resonance of Fe_8Br_8

The unpaired electron density in Fe_8Br_8 was probed by ^{81}Br NMR to determine the spin distribution on the Br^- counterions. Figure 1 shows the ^{81}Br NMR spectrum of Fe_8Br_8 at 280 K with an 8.5 T Zeeman field applied along the intermediate axis of an Fe_8Br_8 single crystal. Two distinct Br sites are present in the Fe_8Br_8 crystal structure at 280 K, as evidenced by the spectrum given in Fig. 1. The intense, narrow peak at 280 K has been preliminarily assigned to the seven bound bromines in the crystal structure of $\{[\text{Fe}_8(\mu_3\text{-O})_2(\mu_2\text{-OH})_{12}(\text{tacn})_6]\text{Br}_7 \cdot \text{H}_2\text{O}\}^+[\text{Br} \cdot 8\text{H}_2\text{O}]^-$ due to relative intensity considerations and the assumed similar magnetic environments at high temperatures of the seven bound bromine nuclei. A significant shift from the Larmor frequency (98.1988 MHz) for the seven bound Br nuclei is noted in all of the ^{81}Br NMR spectra. Figure 2 shows ^{81}Br NMR spectra at 225 K as a function of angle. As is evidenced in all of the spectra taken at 225 K, the large single peak seen at 280 K begins to broaden and split into at

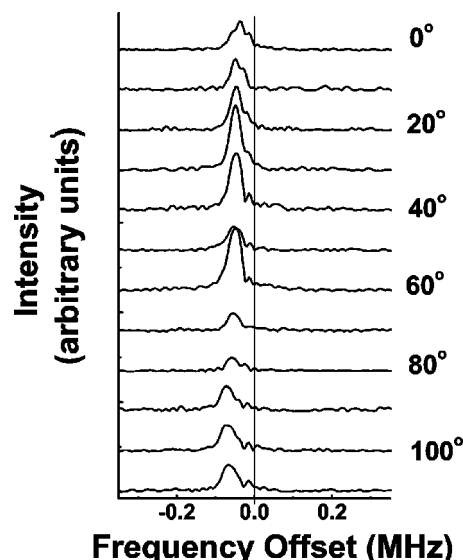


FIG. 2. ^{81}Br NMR spectra of Fe_8Br_8 at 225 K as a function of angle. The zero degree spectrum corresponds to the applied field being approximately along the intermediate axis, while the 90° spectrum corresponds to the approximate hard axis.

least three different peaks. Individual peak assignments have not been carried out to this point, save the unbound Br, but the spectral evolution with lowering temperature is indicative of differing magnetic environments for the individual bound Br nuclei.

Though determination of the magnitude of the frequency shift as a function of angle was not possible due to the rather large linewidths and relatively small frequency shifts, angular dependent studies have yielded an isotropic shift in the average peak position of the seven bound ^{81}Br nuclei. As the magnetic field orientation was changed over a range of 110° , encompassing the intermediate and hard magnetic axes, the average peak position of the seven bound ^{81}Br nuclei did not reach the value of the Larmor frequency. The resonant frequency would be expected to coincide with the Larmor frequency for at least one orientation over a given 90° span if the shift was purely dipolar in origin. In order to calculate the isotropic component of the Larmor frequency offset, a weighted average shift, -0.05121 MHz, was determined for nine orientations. The isotropic shift was used, with the magnetization of Fe_8Br_8 at 225 K (8305 emu/mol), to determine the Fermi contact coupling constant, A_c , through Eq. (1),

$$\Delta \nu / \nu = -A_c \langle S_z \rangle / g_n \mu_n H. \quad (1)$$

In order to obtain an estimate of the electron density present on the bound Br nuclei, the calculated coupling constant, 0.069 MHz, was modelled with an F center in a KBr lattice. The coupling constant from the F center is approximately 25 MHz (Ref. 17) for the 12 Br present in the second shell of the lattice. The ratio (0.00276) of the measured coupling constant (0.069 MHz) to the coupling constant of the F center (25 MHz) yields the approximate unpaired electron density of 0.3% on the seven bound bromines in Fe_8Br_8 .

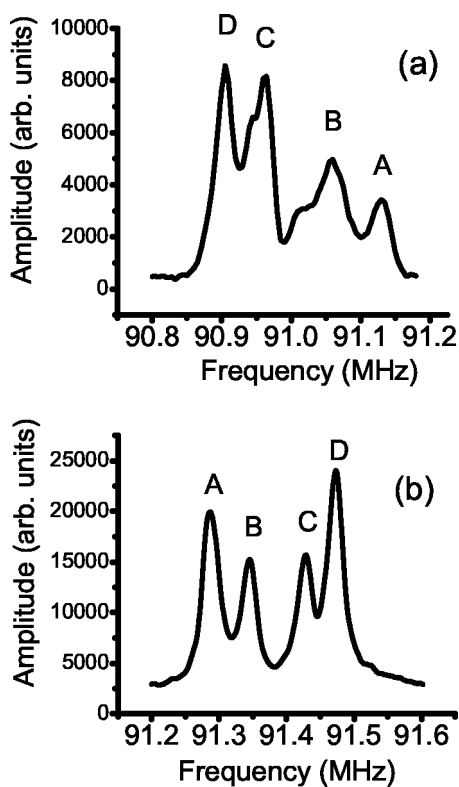


FIG. 3. ^{13}C NMR spectrum of (a) methyl carbons and (b) carbonyl carbons in $\text{Mn}_{12}\text{-Ac}$ with $H\parallel z$.

B. ^{13}C nuclear magnetic resonance of $\text{Mn}_{12}\text{-Ac}$

The ^{13}C NMR spectrum of the aligned samples was measured at room temperature as a function of the orientation of the alignment (easy) axis of the samples with respect to the applied 8.5 T magnetic field. The spectrum at the alignment axis parallel to the applied magnetic field for the methyl carbon labeled sample (a) and the carbonyl carbon labeled sample (b) is shown in Fig. 3. In the case of the methyl carbon labeled sample, the spectrum shows four peaks, one at the free resonance frequency for ^{13}C , and three shifted peaks, with one peak shifted to higher frequency and the other two peaks shifted to lower frequency. The spectrum of the carbonyl carbon labeled sample shows four peaks as well, with one peak unshifted and three peaks shifted to higher frequency. The peaks in both spectra can be assigned

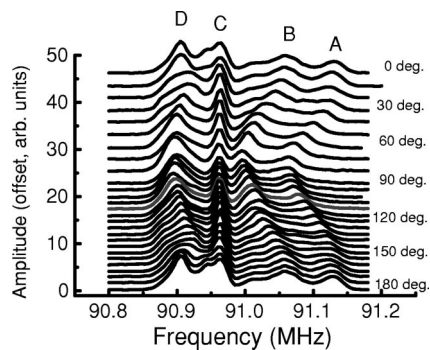


FIG. 4. Angular dependence of the ^{13}C NMR shift of the methyl carbons in $\text{Mn}_{12}\text{-Ac}$.

TABLE I. Electron density on carbonyl and methyl carbons in $\text{Mn}_{12}\text{-Ac}$.

Peak	Isotropic field (Oe)	Dipolar field (Oe)	Calculated dipolar field (Oe μ_B^{-1})	Spin density (% of an electron)
B (carbonyl)	-26.5	11.9	198.2	0.686
C (carbonyl)	172.6	-22.0	-259.3	4.43
D (carbonyl)	230.1	-35.0	-457.0	5.92
A (methyl)	140.0	20.9	448.1	3.59
B (methyl)	65.4	19.6	68.2	1.69
D (methyl)	-32.7	14.1	-120.6	0.840

to specific classes of carbon sites in the $\text{Mn}_{12}\text{-Ac}$ molecule. The orientation dependence of the ^{13}C spectrum of the methyl carbon labeled sample is shown in Fig. 4. The unshifted peak is stationary with respect to orientation, while the three shifted peaks show a disregard dependence. The angular dependence of the ^{13}C spectrum of the carbonyl carbon labeled sample shows similar behavior, with one stationary unshifted peak and three shifted peaks that show orientation dependence. The orientation dependence of the position of the shifted peaks can be fit to a model of a dipolar shift plus an isotropic shift. The isotropic shift can be attributed to electron spin delocalization onto the specific carbon site to which each peak corresponds. Using the hyperfine coupling constant extracted from the temperature dependence of the magnetic susceptibility of $\text{Mn}_{12}\text{-Ac}$, the experimentally determined isotropic field can then be converted into an electron spin density on the carbon sites. These results are given in Table I, and show that there is electron spin delocalization onto the acetate ligands in $\text{Mn}_{12}\text{-Ac}$.

IV. DETERMINATION OF THE ENERGETIC LOCATION AND SPIN HAMILTONIAN PARAMETERS OF THE $S=9$ EXCITED STATE IN Fe_8Br_8

The knowledge of the location of excited states, such as $S=9$, has been an important missing factor in our understanding of the structure and bonding of $\text{Mn}_{12}\text{-Acetate}$ and Fe_8Br_8 . The importance of this can be noted from the fact that for Fe_8Br_8 , the set of spin exchange constants J 's, has not been uniquely determined.¹⁸ Figure 5 (middle panel) shows the experimental EPR spectrum of Fe_8Br_8 at 131 GHz with the Zeeman field applied along the easy axis of an Fe_8Br_8 single crystal at 35 K. As previously shown,¹⁹⁻²² the spectrum consists of a series of strong peaks, hereby labeled α_i , corresponding to the M_s level from which the transition originates in the $S=10$ manifold. The spin Hamiltonian parameters for the $S=10$ state have been previously well established.^{19,20,23,24} In addition to the α transitions, a series of peaks, labeled β_i , is also evident in the spectrum given in Fig. 5. These peaks correspond to $\Delta M_s = \pm 1$ transitions in the $S=9$ excited state of Fe_8Br_8 and are the first definitive experimental evidence of the $S=9$ manifold.

In order to quantitatively analyze the β peaks, they needed to be separated from the α transitions. Gaussian functions were used to fit both the α and β transitions, yielding individual spectra for each manifold. We next analyzed for the origin of the β peaks. As the temperature rises from 5 to

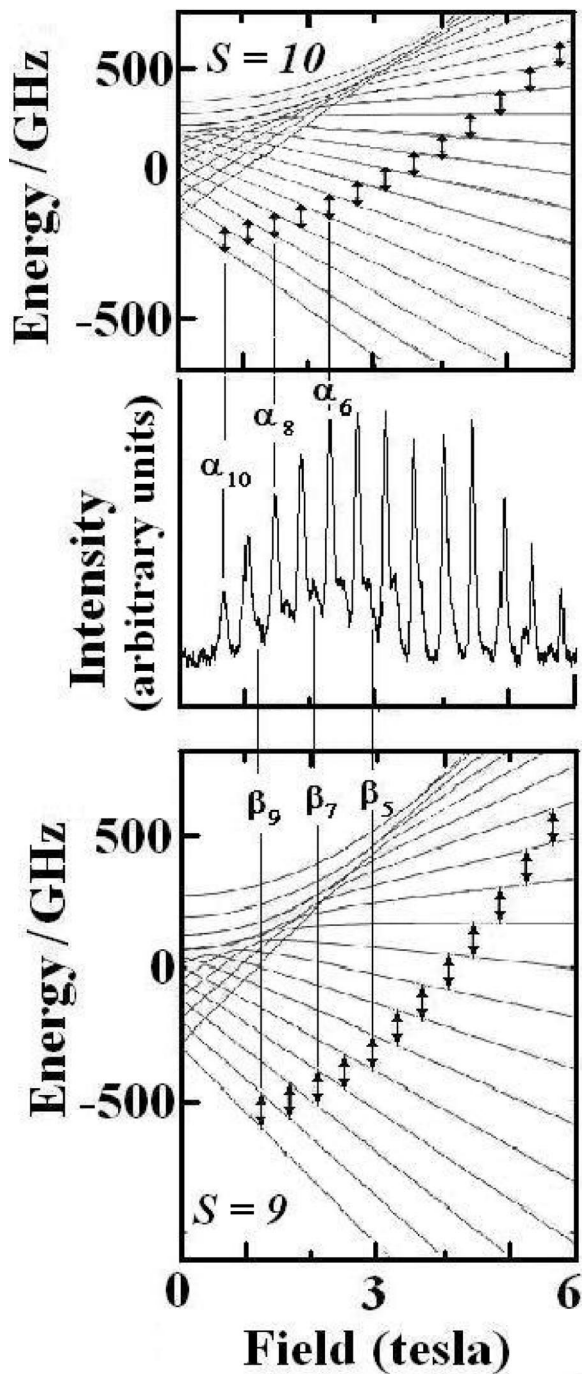


FIG. 5. Energy level diagram for the $S=10$ state (top panel). Experimental EPR spectrum of Fe_8Br_8 for $H\parallel z$ at 35 K and 131 GHz (middle panel). Energy level diagram for the $S=9$ excited state in Fe_8Br_8 (bottom panel).

35 K, the β transitions increase in intensity, though the low field transitions go through a maximum, as would be expected for a multilevel spin system. This temperature dependent intensity of the β spectra unambiguously designates them as being due to a thermally populated excited state.²⁵ The spectral envelopes for the α and β spectra are similar for all of the temperatures studied, though they are slightly modified due to the differing matrix elements in the transition probabilities between the two systems, $P_{nm} \propto |\langle \psi_n | S_+ | \psi_m \rangle|^2$, as shown in Eq. (2),

$$P \propto [S \times (S+1) - M_s \times (M_s+1)]. \quad (2)$$

Once the origin of the β peaks was established, the spin multiplicity, S , of the excited state had to be determined. We noted that the presence of an excited magnetic state with $S=9$ has been previously mentioned in the theoretical studies of Raghu *et al.*,²⁶ as well as by Delfs *et al.*,¹⁸ though no direct experimental evidence has been previously shown. As is evident in all of the spectra, the spectrum in Fig. 5 does not show any sign of a β peak between the α_{-10} and α_{-9} peaks, as would be expected if the β transitions arose from a $S=10$ manifold. Furthermore, the α_{-10} shows a clear Gaussian shape, as would be expected for an individual, well separated, inhomogeneously broadened, low-field EPR peak for Fe_8Br_8 .²⁷

Further evidence that the spin multiplicity of the excited state is $S=9$ is given by the field vs frequency plots and simulated spectra shown earlier.²⁵ The spin Hamiltonian parameters of the $S=9$ state were determined using the simulation program SIM.²⁸ Due to the number of factors affecting line shape, the only optimized parameter in these simulations was peak position, thus preventing us from performing a least squares fitting procedure on the simulated spectra. The separated β spectra were accurately simulated using three different experimental frequencies (110, 131, and 155 GHz) beginning with the same spin Hamiltonian parameters as for the $S=10$ state, with $S=9$, and modifying them to obtain the best visual fit. By using our multifrequency approach, we were able to accurately determine the spin Hamiltonian parameters of the excited state, while confirming its multiplicity as $S=9$. The g value for the $S=9$ state (2.02) is slightly larger than that for the $S=10$ state (2.00), while the D parameter for the $S=9$ state falls in magnitude from that of the $S=10$ state (-0.292 K) by 8% to -0.27 K. Further, the E parameter increases in magnitude from the $S=10$ state (0.047 K) to ± 0.05 K (± 0.015 K). Surprisingly, the B_4^0 parameter for the $S=9$ state is similar in magnitude, -1.3×10^{-6} K, but opposite in sign to the $S=10$ parameter (1.01×10^{-6} K). The off-diagonal fourth order terms, B_4^4 and B_4^2 , were not included in the simulations because all of the experimental spectra were taken along the easy axis of magnetization. Angular dependent studies are currently underway to determine these fourth order terms and further refine the spin Hamiltonian parameters previously given. Energy level diagrams for both the $S=10$ and $S=9$ regimes, including transitions at 131 GHz are shown in Fig. 5, along with the experimental spectrum at 35 K and 131 GHz. In order to determine the energetic position of the $S=9$ excited state, the β peaks were normalized to their corresponding α transitions. The intensity of an EPR transition is given by Eq. (3),

$$I \propto P(N_{M_s} - N_{M_{s+1}})/Z, \quad (3)$$

where P_{nm} is the transition probability as given in Eq. (2), and N_i represents the population of the i th level. Therefore, assuming the partition function, Z , for Fe_8Br_8 is very similar for a given M_s transition in both the $S=9$ and $S=10$ states, the ratio of their intensities is given by Eq. (4),

$$I_9/I_{10} = (P_9/P_{10}) \exp(-\Delta E_{10-9}/kT). \quad (4)$$

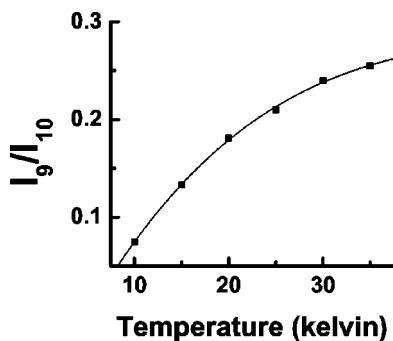


FIG. 6. Boltzmann plot of the normalized ratio of the $M_s = -8$ to $M_s = -7$ transitions. The Boltzmann fit through the data points gives the excitation energy as 18 ± 2 K (see text).

The energetic position of the $S=9$ state was determined by way of a Boltzmann analysis, as shown in Fig. 6. The zero field splitting between the $M_s = \pm 10$ and $M_s = \pm 9$ states (5.5 K) was then added to the energy determined from the Boltzmann analysis to place the $S=9$ state at 24 ± 2 K above the $S=10$ ground state.

V. CONDUCTIVITY MEASUREMENTS

For any optoelectronic applications of a SMM, one must know their charge transport properties. However, until very recently, there was a complete lack of such information on $\text{Mn}_{12}\text{-Ac}$ and Fe_8Br_8 . North *et al.*²⁹ were the first to carry out electric conductivity measurements on $\text{Mn}_{12}\text{-Ac}$ and Fe_8Br_8 and the following is an account based on that study.

A. Conductivity of $\text{Mn}_{12}\text{-acetate}$

The temperature dependence of the resistance for the SMM $\text{Mn}_{12}\text{-Ac}$ was measured with a standard four-probe technique at either constant current or constant voltage. At room temperature, in the constant current configuration, the resistivity values are on the order of $10^9 \Omega \text{ cm}$ and increase in an activated manner upon cooling of the sample as shown in Fig. 7. The arrows indicate the direction of temperature change for the system. Initially, the resistance of Mn_{12} was measured as the sample was cooled to 77 K with liquid nitrogen. Below about 200 K, the resistance of the sample became too high to measure. The sample was warmed by evaporating the coolant and measurements were again initi-

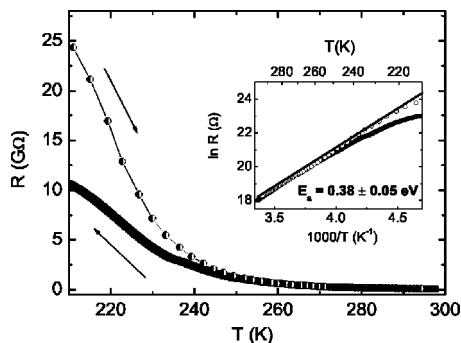


FIG. 7. Temperature dependence of the resistance under conditions of constant current.

ated around 150 K. The saturation of the resistance is an artifact of the setup and our inability to measure extremely high resistances. When the temperature of the $\text{Mn}_{12}\text{-Ac}$ reached about 210 K the resistance began to drop continually up to 300 K. The cause of the irreversibility in the system is still not completely understood. It has tentatively been ascribed to thermally induced defects and/or lattice strain.

Due to the loss of Ohmic equilibrium at lower temperatures, our Arrhenius analysis was limited to temperatures in the 200–300 K range. Figure 7 shows that in this interval, $\ln R$ exhibits a linear dependence when plotted as a function of T^{-1} . This is characteristic of a semiconducting system with a well defined band gap where $R(T) \sim \exp(E_a/k_B T)$ and E_a is the thermal activation energy. From the slope of the line, E_a is estimated to be about 0.38 ± 0.05 eV. Similar activated behavior has been shown through the constant voltage measurements.²⁹ As the temperature of the sample is decreased, the current flow also rapidly decreases and becomes immeasurable below 210 K. The value of E_a from the slope of the linear dependence yields of the Arrhenius plot gives a value of 0.36 ± 0.05 eV.²⁹ For a semiconductor E_a is related to the optical gap E_g by $E_g = 2 E_a$.³⁰ E_g , from the present conductivity measurements, is $0.74 \text{ eV} \pm 0.01 \text{ eV}$. Previous optical experiments by Oppenheimer *et al.* have estimated this value to be 1.08 eV for minority spin cluster, and 1.75 eV for the majority spin cluster.³¹

B. Conductivity of Fe_8Br_8

Temperature dependence studies of single crystals of Fe_8Br_8 were also carried out in the constant current configuration. As shown earlier,²⁹ the temperature dependence of the resistance gives linear Arrhenius behavior, as is the case in $\text{Mn}_{12}\text{-Ac}$. The slope of the line yields an $E_a = 0.73 \pm 0.1$ eV. This would correspond to an E_g value of 1.46 ± 0.2 eV.

VI. SUMMARY AND FUTURE DIRECTIONS

The above discussion points to some new and perhaps unexpected properties of two of the most thoroughly characterized SMMs, $\text{Mn}_{12}\text{-Ac}$ and Fe_8Br_8 . First, while these compounds exhibit semiconductivity as well as photoconductivity, it is clear that the conductivity is very low. Second, it is shown that variable frequency, single crystal, high field EPR spectroscopy, is a unique tool for characterizing the excited states of Fe_8Br_8 and likely also for $\text{Mn}_{12}\text{-Ac}$ and related SMMs. The strong evidence for the existence of the $S=9$ state for Fe_8Br_8 at 24 K should help to settle the long-standing question regarding the set of the exchange constants for this system, and opens new avenues for more precise electronic structure calculations. Third, the NMR evidence for the distribution of the unpaired electron spin density opens up new avenues for understanding the nature of the dipolar fields and hence the mechanism of magnetization tunneling in these materials.

ACKNOWLEDGMENTS

The authors would like to thank the National Science Foundation (NIRT Grant No. DMR 0103290) for financial

support. S.H. would like to thank the NSF, DMR (0196430 and 0239481), and Research Corporation for funding. J.S.B. would like to thank the NSF, DMR Grant No. 023532, and DARPA for funding.

- ¹G. Christou, D. Gatteschi, D. Hendrickson, and R. Sessoli, *MRS Bull.* **25**, 66 (2000).
- ²D. Gatteschi and R. Sessoli, *Angew. Chem., Int. Ed. Engl.* **42**, 268 (2003).
- ³J. R. Friedman, M. P. Sarachik, J. Tejada, and R. Ziolo, *Phys. Rev. Lett.* **76**, 3830 (1996).
- ⁴C. Sangregorio, T. Ohm, C. Paulsen, R. Sessoli, and D. Gatteschi, *Phys. Rev. Lett.* **78**, 4645 (1997).
- ⁵J. A. A. J. Perenboom, J. S. Brooks, S. Hill, T. Hathaway, and N. S. Dalal, *Phys. Rev. B* **58**, 330 (1998).
- ⁶S. Hill, R. S. Edwards, S. I. Jones, N. S. Dalal, and J. M. North, *Phys. Rev. Lett.* **90**, 217204 (2003).
- ⁷R. Sessoli, D. Gatteschi, A. Caneschi, and M. A. Novak, *Nature (London)* **365**, 141 (1993).
- ⁸M. R. Cheesman, V. S. Oganessian, R. Sessoli, D. Gatteschi, and A. J. Thompson, *Chem. Commun. (Cambridge)* **17**, 1677 (1997).
- ⁹E. M. Chudnovsky and J. Tejada, *Macroscopic Quantum Tunneling of the Magnetic Moment* (Cambridge University Press, Cambridge, 1998).
- ¹⁰S. Hill, R. S. Edwards, N. Aliaga-Alcalde, and G. Christou, *Science* **302**, 1015 (2003).
- ¹¹T. Lis, *Acta Crystallogr., Sect. B: Struct. Crystallogr. Cryst. Chem.* **36**, 2042 (1980).
- ¹²K. Weighardt, K. Pohl, I. Jibril, and G. Huttner, *Angew. Chem., Int. Ed. Engl.* **23**, 77 (1984).
- ¹³R. M. Achey, P. L. Kuhns, A. P. Reyes, W. G. Moulton, and N. S. Dalal, *Phys. Rev. B* **64**, 064420 (2001).
- ¹⁴R. M. Achey, P. L. Kuhns, A. P. Reyes, W. G. Moulton, and N. S. Dalal, *Solid State Commun.* **121**, 107 (2002).
- ¹⁵W. G. Clark, M. E. Hanson, F. Lefloch, and P. Segransan, *Rev. Sci. Instrum.* **66**, 2453 (1995).
- ¹⁶(a) S. Hill, J. A. A. J. Perenboom, N. S. Dalal, T. Hathaway, T. Stalcup, and J. S. Brooks, *Phys. Rev. Lett.* **80**, 2453 (1998); (b) M. Mola, S. Hill, P. Goy, and M. Gross, *Rev. Sci. Instrum.* **71**, 186 (2000).
- ¹⁷J. A. Weil, J. R. Bolton, and J. E. Wertz, *Electron Paramagnetic Resonance* (Wiley-Interscience, New York, 1994).
- ¹⁸C. Delfs, D. Gatteschi, L. Pardi, R. Sessoli, K. Weighardt, and D. Hanke, *Inorg. Chem.* **32**, 3099 (1993).
- ¹⁹K. Park, M. A. Novotny, N. S. Dalal, S. Hill, and P. A. Rikvold, *Phys. Rev. B* **65**, 014426 (2002).
- ²⁰A. L. Barra, D. Gatteschi, and R. Sessoli, *Chem.-Eur. J.* **6**, 1608 (2000).
- ²¹E. del Barco, J. M. Hernandez, J. Tejada, N. Biskup, R. Achey, I. Rutel, N. S. Dalal, and J. S. Brooks, *Phys. Rev. B* **62**, 3018 (2000).
- ²²R. Blinc, P. Cevc, D. Arcon, N. S. Dalal, and R. M. Achey, *Phys. Rev. B* **63**, 212401 (2001).
- ²³R. Caciuffo, G. Amoretti, A. Murani, R. Sessoli, A. Caneschi, and D. Gatteschi, *Phys. Rev. Lett.* **81**, 4744 (1998).
- ²⁴A. Mukhin, B. Gorshunov, M. Dressel, C. Sangregorio, and D. Gatteschi, *Phys. Rev. B* **63**, 214411 (2001).
- ²⁵D. Zipse, J. M. North, N. S. Dalal, S. Hill, and R. S. Edwards, *Phys. Rev. B* **68**, 184408 (2003).
- ²⁶C. Raghu, I. Rudra, D. Sen, and S. Ramasesha, *Phys. Rev. B* **64**, 064419 (2001).
- ²⁷S. Hill, S. Maccagnano, K. Park, R. M. Achey, J. M. North, and N. S. Dalal, *Phys. Rev. B* **65**, 224410 (2002).
- ²⁸Simulation software by Dr. H. Weihe; for more information see <http://sophus.kiku.dk/software/epr/epr.html>
- ²⁹J. M. North, D. Zipse, N. S. Dalal, E. S. Choi, E. Jobiliong, J. S. Brooks, and D. L. Eaton, *Phys. Rev. B* **67**, 174407 (2003).
- ³⁰C. Kittel, *Introduction to Solid State Physics* (Wiley-Interscience, New York, 1986).
- ³¹S. M. Oppenheimer, A. B. Sushkov, J. L. Musfeldt, R. M. Achey, and N. S. Dalal, *Phys. Rev. B* **65**, 054419 (2002).